

Harmonizing SO(3)-Equivariance with Neural Expressiveness: a Hybrid Deep Learning Framework Oriented to the Prediction of Electronic Structure Hamiltonian

Shi Yin^{a,*}, Xinyang Pan^b, Xudong Zhu^{a,b}, Tianyu Gao^b, Haochong Zhang^a,
Feng Wu^{a,b}, *Fellow of IEEE*, and Lixin He^{a,b,*}, *Fellow of IOP*

^a*Institute of Artificial Intelligence, Hefei Comprehensive National Science Center*

^b*University of Science and Technology of China*

Abstract

Deep learning for predicting the electronic structure Hamiltonian of quantum systems necessitates satisfying the covariance laws, among which achieving SO(3)-equivariance without sacrificing the non-linear expressive capability of networks remains unsolved. To navigate the harmonization between equivariance and expressiveness, we propose a deep learning method, namely Har-moSE, synergizing two distinct categories of neural mechanisms as a two-stage cascaded regression framework. The first stage corresponds to group theory-based neural mechanisms with inherent SO(3)-equivariant properties prior to the parameter learning process, while the second stage is characterized by a non-linear 3D graph Transformer network we propose featuring high capability on non-linear expressiveness. The novel combination lies in the point that, the first stage predicts baseline Hamiltonians with abundant

*Corresponding authors

Email addresses: shiyin@iaai.ustc.edu.cn (Shi Yin), helx@ustc.edu.cn (and Lixin He)

SO(3)-equivariant features extracted, assisting the second stage in empirical learning of equivariance; and in turn, the second stage refines the first stage’s output as a fine-grained prediction of Hamiltonians using powerful non-linear neural mappings, compensating for the intrinsic weakness on non-linear expressiveness capability of mechanisms in the first stage. Our method enables precise, generalizable predictions while maintaining robust SO(3)-equivariance under rotational transformations, and achieves state-of-the-art performance in Hamiltonian prediction on six benchmark databases.

Keywords: Deep Learning, Neural Networks, AI for Science, Atomic Simulation, 3D Graphic Modeling

1. Introduction

Recently, deep learning methods [19, 21, 7, 13, 27, 6] have emerged as a promising trend for predicting the electronic structure Hamiltonian, an essential physical quantity in understanding a wide range of properties, including electronic structures, magnetic properties, optics, transport, and numerous other properties. These methods have demonstrated great potentials in terms of prediction accuracy and offer a way to bypass the computationally exhaustive self-consistent steps of the traditional Density Functional Theory (DFT) method [9, 11], thereby providing a viable pathway for the effective simulation and design of large-scale atomic systems, laying the foundation for many down-stream applications [24], particularly in the development of hardware devices that are critical for information processing, storage, and computation.

However, applying deep learning techniques to the Hamiltonian prediction

task continues to present substantial challenges, highlighting the evolving demands on deep learning technology. An ultra-high accuracy to 10^{-1} meV scale (10^{-4} eV) is required to precisely calculate the down-stream physical quantities such as band structures. Furthermore, the fidelity of Hamiltonian predictions should not be confined to a specific coordinate system; rather, the results must demonstrate robust symmetry and generalizability across various choices of reference frames. This necessitates that deep learning methods capture the intrinsic symmetries of the Hamiltonian with respect to transformations of the coordinate system, ensuring the consistency with physical principles covariant to these transformations. In the context of Hamiltonian prediction, the key covariance principles are 3D translational invariance and rotational equivariance. By utilizing relative coordinates, 3D translational invariance has been effortlessly achieved, while 3D rotational equivariance, i.e., equivariance to the $SO(3)$ group, remains a challenging target to guarantee. This difficulty arises because the Hamiltonian of each pair of atoms is usually high-dimensional, and its variation space under rotational disturbance is large. Consequently, it is difficult to cover the vast variability space they inhabit merely depending on parameter learning from discrete training samples. To address this, several works [27, 6] applied group theory-guaranteed feature descriptors and tensor operators assuring inherent $SO(3)$ -equivariance prior to the data-driven parameter learning process. However, to guarantee such $SO(3)$ -equivariance independent to specific network parameters, these methods highly restricted the use of non-linear activation layers for $SO(3)$ -equivariant features, i.e. those with degrees greater than 0. Given that the expressiveness capability of modern deep networks heavily relies on the

extensive use of non-linear mappings, this restriction resulted in a significant drawback on network’s expressiveness capabilities. This, in turn, led to bottlenecks in fitting complex mappings, limiting the accuracy achievable in predicting Hamiltonians. This dilemma, is also broadly prevalent in other 3D machine learning tasks where $SO(3)$ -equivariance is highlighted, as analyzed by Zitnick *et al.* [28].

To harmonize $SO(3)$ -equivariance and expressiveness for the prediction of electronic structure Hamiltonians, this paper proposes a novel two-stage regression framework, namely HarmoSE, which combines mechanisms boasting parameter-independent, prior $SO(3)$ -equivariance with mechanisms featuring flexibility in non-linear expressiveness, overcoming the respective challenges of each categories of mechanisms, i.e., the limited non-linear expressive capability for the former as well as the difficulty of learning $SO(3)$ -equivariance from data for the latter, through effective complementary strategies. Specifically, the first regression stage corresponds to the neural mechanisms constructed based on group theory with prior equivariant properties of 3D atomic systems, predicting an approximate value of the Hamiltonian, with abundant $SO(3)$ -equivariant features provided. In the second stage, a highly expressive graph Transformer network we design, with no restrictions on non-linear activations, takes over. This network dynamically learns the 3D structural patterns of the atomic systems, compensates for the expressiveness shortcomings of the first-stage network arising from limited non-linear mappings, and refines the Hamiltonian values predicted in the first stage to enhance accuracy. Although this stage might not possess a parameter-independent prior $SO(3)$ -equivariance due to its non-linearity, it is

capable of capturing $\text{SO}(3)$ -equivariance through learning effective network parameters via the help of three pivotal mechanisms. First, instead of directly regressing the entire Hamiltonians, the second stage aims to refine the Hamiltonian predictions from the first stage with corrective adjustments in a cascaded manner. The scopes of adjustments are smaller, lowering down the difficulties on non-linear learning of $\text{SO}(3)$ -equivariance. Second, the second-stage network incorporates covariant features, including $\text{SO}(3)$ -equivariant features extracted by the first-stage network and $\text{SO}(3)$ -invariant features engineered by geometric knowledge, with its inputs to assist in the implicit learning of $\text{SO}(3)$ -equivariance. Third, as the core of Transformer, the attention mechanism has potentials to adapt to geometric condition variations such as coordinate transformations, through its dynamic weighting strategy. Collectively, the combination of the two categories of neural mechanisms in the two stages allows the framework to overcome the challenges of each individual mechanism and make precise, generalizable, and $\text{SO}(3)$ -equivariant predictions, being much more effective than simply increasing the parameter count for the network from one stage and fine-tuning it alone.

Our contributions are summarized below:

- Our work explores new deep learning paradigm with the synergy of two categories of distinct neural mechanisms, where the first one exhibits prior equivariance independent of parameter learning, and the second one possesses ample non-linear expressiveness, overcoming the respective challenges each mechanism faces via fully releasing their complementarity, and successfully harmonizing $\text{SO}(3)$ -equivariance with neural expressiveness.
- We design a Transformer architecture within the proposed framework,

incorporating advanced mechanisms such as covariant feature integration and multi-head attentions, enabling effective modeling of diverse 3D atomic structures with $SO(3)$ -equivariant properties.

- Our method achieves state-of-the-art (SOTA) performance on Hamiltonian regression in six benchmark databases, showing good potential on simulating diverse categories of atomic systems. Particularly, our SOTA performance in the twisted samples, which exhibit $SO(3)$ -equivariance effects due to the inter-layer rotations, comprehensively confirm the strong capability in capturing the intrinsic $SO(3)$ -equivariance of Hamiltonians. The materials consisted in these databases have extensive values in the realm of information technology, implicating an applicable potential of our method in advancing the development and optimization of information hardware.

2. Related Work

In this part, we firstly overview deep learning studies on capturing rotational equivariance. After that, we segue into related works on deep Hamiltonian prediction, in which 3D rotational equivariance is pursued.

As representative researches on equivariance to discrete rotational group, Dieleman *et al.* [3] introduced cyclic symmetry operations into CNNs to achieve rotational equivariance; Ravanbakhsh *et al.* [18] explored parameter-sharing techniques for equivariance to discrete rotations; Kondor *et al.* [12] developed equivariant representations via compositional methods and tensor theory; Zitnick *et al.* [28], Passaro *et al.* [17] and Liao *et al.* [15] introduced spherical harmonic bases for atomic modeling, focusing on rotational equivariance but limited to discrete sub-groups of $SO(3)$ due to their sampling strategy. These approaches were very effective on discrete symmetries

but sub-optimal on handling continuous 3D rotations. Focusing on equivariance to continuous rotational group, Jaderberg *et al.* [10] and Cohen *et al.* [2] achieved considerable success in 2D image recognition tasks by modeling equivariance to in-plane rotations. However, their applications were limited within the scope of 2D tasks and did not fit for the more complex demands of equivariance to 3D continuous rotational group, i.e. $SO(3)$, required in the Hamiltonian prediction task.

In the field of researches on equivariance to $SO(3)$, approaches like DeepH [13] explored equivariance via a local coordinate strategy, which made inference within the fixed local coordinate systems built with neighboring atoms, then transferred the output according to equivariance rules to the corresponding global coordinates. However, due to a lack of in-depth exploration of $SO(3)$ -equivariance at the neural mechanism level, this method faced challenges when the local coordinate system underwent rotational disturbances from non-rigid deformation, e.g. the inter-layer twist of bilayer structures. In contrast, some methods [20, 4, 5] considered $SO(3)$ -equivariance from the perspective of intrinsic mechanisms of neural networks, developed group theory-informed equivariant operations, such as linear scaling, element-wise sum, direct sum, direct product, as well as the Clebsch-Gordan decomposition, effectively applying in tasks like molecular dynamics simulation [16, 14] and Hamiltonian prediction [19, 21, 6], where DeepHE3 [6] was validated as a SOTA method across diverse atomic systems. However, a common challenge across these methods lies in the fact that, to achieve inherent equivariance prior to the parameter learning process, they forbade the use of complex non-linear mappings like *Sigmoid*, *SiLU*, and *Softmax*

for $\text{SO}(3)$ -equivariant features, significantly limiting the network’s expressive potential and creating a bottleneck in generalization performance. Although these approaches tried to enhance expressiveness via a gated activation function, where $\text{SO}(3)$ -invariant features undergone through non-linear activation layers were used as gating coefficients that were multiplied with $\text{SO}(3)$ -equivariant features, this mechanism, viewed from the perspective of equivariant features, amounted to a linear operation and did not fundamentally improve their expressive capability. For these methods, this equivariance-expressiveness dilemma remains an unsolved problem.

3. Preliminary

In the study of symmetry on mathematical structures, covariance encompasses two fundamental concepts: invariance and equivariance. An operation A is called invariant under another operation B if the result of A remains unchanged when B is applied, formally $A(B(x)) = A(x)$; on the other hand, A is equivariant with respect to B if applying B before or after A has the same effect, expressed as: $A(B(x)) = B(A(x))$. The key covariance properties of Hamiltonians are the 3D translational invariance and rotational equivariance with respect to reference frame. Since 3D translational invariance can be easily achieved by using the relative coordinates between two atoms, the focus here should be on studying equivariance to $\text{SO}(3)$, i.e. a group consisting of all continuous 3D rotation operations. In the context of Hamiltonians, when the reference frame rotates by a rotation matrix denoted as \mathbf{R} , the edge of an atom pairs (i, j) transforms from \mathbf{r}_{ij} to $\mathbf{R} \cdot \mathbf{r}_{ij}$, and the Hamiltonians in the direct sum state transforms equivariantly from \mathbf{h}_{ij} to $D(\mathbf{R}) \cdot \mathbf{h}_{ij}$, where $D(\mathbf{R})$ is the Wigner-D matrix. Note that here we present $\text{SO}(3)$ -equivariance

under the direct sum state due to its simple vector form. For the equivalent formulation under the matrix-formed direct product state, please refer to Gong *et al.* [6].

The requirements for the fitting and generalization capability of a neural network $f_{nn}(\cdot)$ for Hamiltonian prediction can be formally expressed as: $f_{nn}(\{\mathbf{r}_{ij}|i \in Nodes, ij \in Edges\}) \cong \{\mathbf{h}_{ij}\}$; moreover, the requirement on SO(3)-equivariance can be represented as: $f_{nn}(\{\mathbf{R} \cdot \mathbf{r}_{ij}|i \in Nodes, ij \in Edges\}) \cong \{D(\mathbf{R}) \cdot \mathbf{h}_{ij}\}$. It is crucial that $f_{nn}(\cdot)$ intrinsically embodies SO(3)-equivariance to effectively generalize under rotational reference frames. An intuitive way to achieve this is data-driven empirical learning, however, this is challenging for the Hamiltonian prediction task, since \mathbf{h}_{ij} , consisting of multiple angular momentums, is typically high-dimensional with a total of dimensions likely reaching into the hundreds or thousands. Moreover, \mathbf{h}_{ij} is not determined in isolation by the types of atom i and j as well as their relative positions; geometric of atoms that interact with them also have complex influences on \mathbf{h}_{ij} . Under thermal motions and rotational disturbances, the high-dimensional \mathbf{h}_{ij} may vary in a vast space, which is difficult to be covered with a finite set of discrete training samples in the learning process. A potential alternative approach is to consider operators that maintain SO(3)-equivariance independent of the learning process from the perspective of group theory. However, as analyzed in Section 2, this approach introduces the limitations on the network’s expressive capabilities. This paper aims to resolve these challenges, achieving a harmonious integration of SO(3)-equivariance and non-linear expressive power in the deep Hamiltonian regression model.

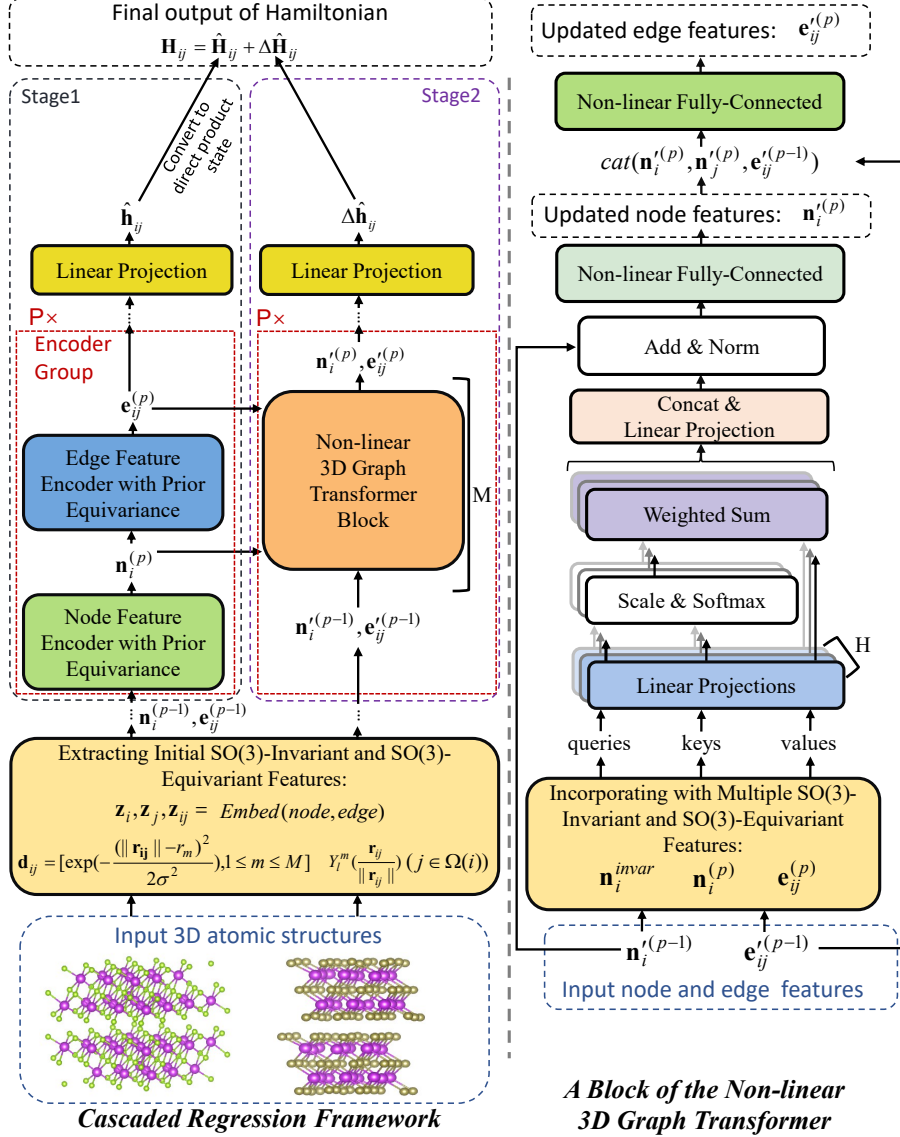


Figure 1: Left part: overview of the two-stage regression framework for Hamiltonian prediction, with the first stage extracting features with prior SO(3)-equivariance independent to the learning process and making baseline predictions, and the second stage enhancing accuracy via advanced non-linear mechanisms. The first-stage network aids the second-stage network in learning SO(3)-equivariance, while the second-stage network compensates for the expressiveness capability of first-stage network. Right part: The internal architecture of the non-linear 3D graph Transformer network.

4. Method

As shown in Fig. 1, to harmonize SO(3)-equivariance and expressiveness for the deep learning paradigm, we propose a novel framework, namely HarMOSE, effectively hybridizing networks in two regression stages, from which the first-stage network, a group theory-informed network possessing SO(3)-equivariance prior to the learning process, provides essential foundations to the second stage in mastering SO(3)-equivariance, whereas the second-stage network, with highly expressive non-linear mappings, enriches the expressiveness capabilities of the whole framework. The combination of these two stages not only enhances expressiveness but also ensures robust equivariance to rotations of reference frames, bringing accurate predictions for electronic structure Hamiltonians despite rotational transformations.

4.1. Initial Features

In our framework, the initial feature for the $i(1 \leq i \leq N)$ th node is its node embedding, denoted as \mathbf{z}_i , a coordinate-independent SO(3)-invariant semantic embedding that marks its element type. Given the locality of the Hamiltonian [13], each atom j in the local set $\Omega(i)$ within the cutoff radius of an atom i form an edge with i . From each edge, a Hamiltonian is defined. The initial features for edge (i, j) include both SO(3)-invariant encodings and SO(3)-equivariant encodings. The former includes edge embeddings \mathbf{z}_{ij} marking the types of interacting atom pairs, as well as the distance features \mathbf{d}_{ij} in the form of Gaussian functions [13]; the latter is spherical harmonics, denoted as $Y_l^m(\frac{\mathbf{r}_{ij}}{\|\mathbf{r}_{ij}\|})$, where $\frac{\mathbf{r}_{ij}}{\|\mathbf{r}_{ij}\|}$ describes the relative orientation between two atoms. Worth noting, a node and itself also possess a Hamiltonian. In other words, $i \in \Omega(i)$ and \mathbf{e}_{ii} also forms a valid edge. In this case, $Y_l^m(\frac{\mathbf{r}_{ij}}{\|\mathbf{r}_{ij}\|})$

cannot be used to calculate directional features and a vector filled with 0 is used as a substitute. The above initial features are used to model the Hamiltonian which obeys SO(3)-equivariance, additionally, these features also inherently fulfill translational invariance with respect to global coordinates, another natural attribute of Hamiltonians.

4.2. The First Regression Stage

In our framework, the primary role of the first regression stage is to extract node and edge representations with intrinsic SO(3)-equivariance independent to network parameters, and regress baseline Hamiltonian predictions, denoted as $\hat{\mathbf{h}}_{ij}$ in the direct sum state and $\hat{\mathbf{H}}_{ij}$ in the direct product state for each pair (i, j) , establishing a firm foundation on SO(3)-equivariance in both feature level and the regression target level. The encoding process of the p -th encoder group can be described by the following equation:

$$\begin{aligned} \mathbf{n}_i^{(p)} &= Gate(\mathbf{n}_i^{(p-1)} + \sum_{j \in \Omega(i)} EquiLin(\mathbf{n}_i^{(p-1)}, \mathbf{e}_{ij}^{(p-1)}, \mathbf{n}_j^{(p-1)})) \\ \mathbf{e}_{ij}^{(p)} &= Gate(EquiLin(\mathbf{n}_i^{(p)}, \mathbf{e}_{ij}^{(p-1)}, \mathbf{n}_j^{(p)})) \end{aligned} \quad (1)$$

where $\mathbf{n}_i^{(p)}$ and $\mathbf{e}_{ij}^{(p)}$ respectively denote the node and edge features from the p th ($1 \leq p \leq P$) encoder group, $Gate(\cdot)$ is the gated activation function introduced in Section 2, $EquiLin(\cdot)$ denotes a combination of tensor operators consisting of linear scaling, element-wise sum, direct sum, direct product, as well as the Clebsch-Gordan decomposition, possessing parameter-independent SO(3)-equivariance guaranteed by group theory. These operators, serving as our first-stage backbone, have been comprehensively developed in previous works [20, 5, 6], achieving maturity in their equivariance

capabilities, yet facing inherent limitations in non-linear expressiveness cannot be easily resolved within their mechanisms. Therefore, we focus more on the complementary mechanisms of the hybrid two-stage regression framework as well as the design of the second-stage network, aiming at rectifying the intrinsic weaknesses in non-linear expressiveness of the first-stage network while embodying robust $\text{SO}(3)$ -equivariant capability.

4.3. The Second Regression Stage

The second regression stage of our framework is designed to fully exploit non-linear mappings to enhance the expressive capability of the whole framework while capturing $\text{SO}(3)$ -equivariance. For that purpose, as shown in the right part of Fig. 1, we propose a 3D graph Transformer which effectively models 3D atomic structures and predicts non-linear correction terms that complement the predictions from the first stage, achieving high-precision Hamiltonian prediction. Yet, one key problem to solve lies that, non-linear projections might not have parameter-independent guarantee on $\text{SO}(3)$ -equivariance, forcing the second stage to capture equivariance through learning effective network parameters from the data. Thus, we must address the difficulty on empirical learning $\text{SO}(3)$ -equivariance of Hamiltonians as discussed in Section 3. Our second-stage network adeptly resolves this issue, simultaneously capturing $\text{SO}(3)$ -equivariance and enhancing the expressive capabilities. This is primarily attributed to three pivotal mechanisms we design.

First, the second regression stage works in a cascaded manner, which means that its prediction target is not the entire Hamiltonian but a correction term $\Delta\hat{\mathbf{H}}_{ij}$, relative to the first stage’s output, i.e. the initial Hamiltonian

estimate $\hat{\mathbf{H}}_{ij}$. The sum of these two stages' outputs forms the final prediction of the Hamiltonian: $\mathbf{H}_{ij} = \hat{\mathbf{H}}_{ij} + \Delta\hat{\mathbf{H}}_{ij}$. Given that the predicted results of $\hat{\mathbf{H}}_{ij}$ are theoretically SO(3)-equivariant and numerically approximate to reasonable, the range of variations for the correction term $\Delta\hat{\mathbf{H}}_{ij}$, becomes smaller compared to $\hat{\mathbf{H}}_{ij}$. This reduces the complexity of the output space for the second stage and enhances the feasibility on implicitly capturing SO(3)-equivariance through data-driven learning for non-linear modules.

Second, several theoretical-guaranteed covariant features, including both SO(3)-equivariant and SO(3)-invariant features, are integrated into the input features of each Transformer block in the second stage to aid it in capturing equivariance, as shown in Eq. (2):

$$\begin{aligned}\tilde{\mathbf{n}}_i^{(p)} &= \mathbf{n}_i'^{(p-1)} + \alpha\mathbf{n}_i^{(p)} + \beta\mathbf{n}_i^{invar}, \\ \tilde{\mathbf{e}}_{ij}^{(p)} &= \mathbf{e}_{ij}'^{(p-1)} + \lambda\mathbf{e}_{ij}^{(p)}\end{aligned}\tag{2}$$

where α , β and λ are hyper-parameters, $\mathbf{n}_i'^{(p-1)}$ and $\mathbf{e}_{ij}'^{(p-1)}$ denote the outputs of the Transformer at the $p-1$ th encoder group, $\tilde{\mathbf{n}}_i^{(p)}$ and $\tilde{\mathbf{e}}_{ij}^{(p)}$ respectively serve as the input node and edge features for the subsequent modules of the Transformer at the p th encoder group, $\mathbf{n}_i^{(p)}$ and $\mathbf{e}_{ij}^{(p)}$ are the SO(3)-equivariant node and edge features, respectively, from the corresponding encoder group of the first-stage network. Besides SO(3)-equivariant features, since as demonstrated by literature [23, 25, 26], SO(3)-invariant features also facilitate the learning of SO(3)-equivariance, we also develop a SO(3)-invariant node feature, i.e., \mathbf{n}_i^{invar} , aggregated from multiple SO(3)-invariant features, such as node embeddings \mathbf{z}_i , edge embeddings \mathbf{z}_{ij} , distance features \mathbf{d}_{ij} , and triplet angle feature θ_{ijk} formed by node i as well as two of its local atoms j and k ,

in the way like:

$$\mathbf{n}_i^{invar} = \sum_{(j,k) \in \Omega(i)} FC(cat(\mathbf{z}_i, \mathbf{z}_j, \mathbf{z}_k, \mathbf{d}_{ij}, \mathbf{d}_{ik}, \mathbf{c}_{ijk})) \quad (3)$$

where $cat(\cdot)$ is the concatenation operator, $FC(\cdot)$ denotes fully-connected layers with non-linear activations, $\mathbf{c}_{ijk} = [\cos(\theta_{ijk}), \cos(\theta_{ijk}), \dots]$ is a vector extended by duplication, which serves to amplify the angle features for $FC(\cdot)$. To reduce the quadratic complexity, i.e., $O(|\Omega(i)|^2)$ when sampling $(j, k) \in \Omega(i)$, we arrange the set $\Omega(i)$ as an array and only extract adjacent element pairs as tuples (j, k) , lowering down the sampling complexity to $O(|\Omega(i)|)$ to efficiently compute \mathbf{n}_i^{invar} . In Eq. (2), \mathbf{n}_i^{invar} is directly merged into node features, and since node features are then merged into edge features in the subsequent modules, it also enhances the learning of edge features. With the help of these covariant features, the second-stage network, even a non-linear one, can also capture the $SO(3)$ -equivariant properties inherent in the Hamiltonian.

Third, we design a multi-head attention mechanism to learn node and edge representations of the 3D atomic systems. The capability to dynamically focus on related geometric features enables robust adaptability to diverse geometric conditions, from structural variants to coordinate transformations. Specifically, the attention mechanism firstly learns dynamic weights, i.e. $\alpha_{ij}^{(p)}$ for the edge (i, j) at the p th encoder group, based on the interactive relationship between the current atom i and its local atoms $j \in \Omega(i)$, as shown

in Eq. (4):

$$\begin{aligned}
\mathbf{q}_{ij}^{h(p)} &= \mathbf{W}_q^h \cdot \text{cat}(\tilde{\mathbf{n}}_i^{(p)}, \tilde{\mathbf{e}}_{ij}^{(p)}), \\
\mathbf{k}_{ij}^{h(p)} &= \mathbf{W}_k^h \cdot \text{cat}(\tilde{\mathbf{n}}_j^{(p)}, \tilde{\mathbf{e}}_{ij}^{(p)}), \\
\alpha_{ij}^{(p)} &= \text{softmax}\left(\frac{(\mathbf{q}_{ij}^{h(p)})^T \cdot \mathbf{k}_{ij}^{h(p)}}{\sqrt{d_h}}\right)
\end{aligned} \tag{4}$$

where $h(1 \leq h \leq H)$ is the head index, d_h is the dimension of features, \mathbf{W}_q^h and \mathbf{W}_k^h are parameter matrices to calculate queries and keys, i.e., $\mathbf{q}_{ij}^{h(p)}$ and $\mathbf{k}_{ij}^{h(p)}$, respectively. Here the scale factor $\sqrt{d_h}$ in the denominator is used to prevent $\text{softmax}(\cdot)$ from gradient saturation, and the multiple heads aim at enchainning the model capacity. Based on $\alpha_{ij}^{(p)}$, the node features are updated flexibly through the structural information embedded in its local sets, as shown in Eq. (5):

$$\begin{aligned}
\mathbf{v}_i^{h(p)} &= \sum_{j \in \Omega(i)} \alpha_{ij}^{(p)} \cdot (\mathbf{W}_v^h \cdot \text{cat}(\tilde{\mathbf{n}}_j^{(p)}, \tilde{\mathbf{e}}_{ij}^{(p)})), \\
\mathbf{n}_i^{(p)} &= FC(LN(\mathbf{W}_o \cdot \text{cat}(\mathbf{v}_i^{1(p)}, \dots, \mathbf{v}_i^{H(p)})) + \mathbf{n}_i^{(p-1)})
\end{aligned} \tag{5}$$

where $LN(\cdot)$ is the layer normalization operator, $FC(\cdot)$ denotes fully-connected layers with non-linear activations. Based on $\mathbf{n}_i^{(p)}$, the edge representations are updated as:

$$\mathbf{e}_{ij}^{(p)} = FC(\text{cat}(\mathbf{n}_i^{(p)}, \mathbf{n}_j^{(p)}, \mathbf{e}_{ij}^{(p-1)})) \tag{6}$$

when repeatedly stacking operations in Eq. (5) and (6) in an alternate manner, local patterns can incrementally spread to a larger scale through the neighbors of neighboring atoms. Nevertheless, given the Hamiltonian’s locality, there’s typically no need for information transfer over very long distances. Finally, the correction term outputted by the second stage is regressed from

the edge features $\mathbf{e}_{ij}^{(P)}$ encoded by the last encoder group, in the way like:

$$\Delta\hat{\mathbf{H}}_{ij} = DStoDP(\Delta\hat{\mathbf{h}}_{ij}) = DStoDP(FC(\mathbf{e}_{ij}^{(P)})) \quad (7)$$

where $DStoDP(\cdot)$ is the conversion operation from the vector-formed direct sum state to the matrix-formed direct product state, which is more commonly used in the down-stream computational tasks based on Hamiltonians.

4.4. Training

Considering that networks from the two stages employ fundamentally different operators, training them simultaneously in a joint manner may pose optimization difficulties. Therefore, we optimize them separately. Denote the ground truth Hamiltonian label for the atom pair (i, j) as \mathbf{H}_{ij}^* , in the first stage, parameters of the first-stage network are optimized by minimizing $MSE(\hat{\mathbf{H}}_{ij}, \mathbf{H}_{ij}^*)$, while in the second stage, parameters of the second-stage network are optimized by minimizing $MSE(\Delta\hat{\mathbf{H}}_{ij}, (\mathbf{H}_{ij}^* - \hat{\mathbf{H}}_{ij}))$. To avoid interference, the networks of the two stages use independent node and edge embeddings; moreover, during the training of the second-stage network, gradients are not propagated back to the first-stage network. Adam is used for optimization.

5. Experiments

5.1. Experimental Conditions

We conduct experiments on six benchmark material databases, including Monolayer Graphene (abbreviated as *MG*), Monolayer MoS2 (*MM*), Bilayer Graphene (*BG*), Bilayer Bismuthene (*BB*), Bilayer Bi2Te3 (*BT*), and Bilayer Bi2Se3 (*BS*), which are released by the DeepH series [13, 6] with CC BY

4.0 license. These databases are diverse and representative, as they cover atomic structures with strong chemical bonds within individual layers and weak vdW interactions between two layers; and include varied degrees of spin-orbit coupling (SOC), featuring both strong SOC samples like *BT*, *BB* and *BS*, and others with weak SOC. These atomic structures hold significant potential and value in the information science and technology sector:

- *MG*, due to its exceptional electrical conductivity and mechanical strength, is ideal for developing next-generation wearable electronic devices and super-capacitors;

- *MM*, due to its semiconducting properties, is perfect for the fabrication of thin-film transistors (TFTs) and photodetectors, promising advancements in display technology and optical communication systems;

- *BG*, by leveraging its tunable bandgap, can be used in the creation of energy-efficient electronic components and sensors, potentially transforming the fields of power generation and environmental monitoring;

- *BB*, offering substantial promise for spintronic devices, which utilize the electron spin state alongside the electronic charge to enhance device performance;

- *BT*, pivotal for constructing robust, high-efficiency thermoelectric devices and sensors, offering new opportunities for enhancing energy conversion technologies and sensitive detection systems.

- *BS*, recognized for its unique topological insulator properties that allow for the manipulation of surface states, is pivotal in the creation of ultra-low power electronics and robust quantum computers, paving the way for breakthroughs in computational efficiency and security.

Table 1: Brief statistics of experimental databases on the sizes of training, validation, and testing sets including both non-twisted samples (nt) and twisted samples (t), as well as the dimensions of the Hamiltonians in the direct sum state for each atom pair.

| | MG | MM | BG | BB | BT | BS |
|--------------------------|-----|-----|-----|-----|------|-----|
| Train (nt) | 270 | 300 | 180 | 231 | 204 | 231 |
| Val (nt) | 90 | 100 | 60 | 113 | 38 | 113 |
| Test (nt) | 90 | 100 | 60 | 113 | 12 | 113 |
| Test (t) | - | - | 9 | 4 | 2 | 2 |
| Dim(\mathbf{h}_{ij}) | 169 | 361 | 169 | | 2888 | |

The training, validation, and testing sets as well as the data pre-processing protocols we use are exactly the same as [6]. A concise overview of these databases is presented in Table 1. For more details, please refer to the original papers of these databases. Predicting the Hamiltonian accurately for these atomic structures poses a significant challenge due to the presence of structural deformations caused by thermal motions and inter-layer twists, as shown in Fig. 2. Worth noting, the twisted structures have become a research hotspot due to their potentials for new electrical and quantum topological properties [1, 22, 8]. During the twist transformations, the relative rotation between atoms and the coordinate system brings the corresponding SO(3)-equivariant effects; meanwhile, the change in orientations between two layers of atoms causes variations in vdW interactions. These combined effects present a challenge to both of the equivariance and expressiveness capabilities of the regressor. In our experiments, the twisted subsets are even challenging as there are no such samples in the training set.

To ensure the reproducibility, we use a fixed random seed, i.e., 42, for

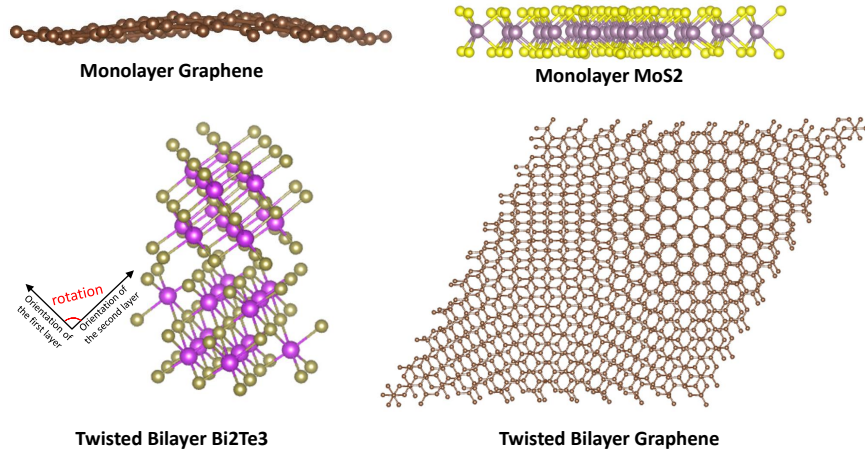


Figure 2: Visualization of challenging testing samples, which exhibit structural deformations caused by thermal motions and inter-layer twists, calling for strong capabilities on expressiveness and $SO(3)$ -equivariance of a regression model.

all procedures involving randomness, such as parameter initialization, data loader, as well as the rigid rotational augmentation introduced during training. Our experiments are conducted on an internal cluster of Tesla A100 servers where 16 cards are used, each with 80 GiB of GPU memory. Except for the network modules we need to compare with, i.e., those from DeepHE3 [6], the hyper-parameters of our framework are determined based on model selection on the validation sets; for DeepHE3, we adopt the optimal hyper-parameters officially provided, as described below. The entire set of hyper-parameters is included in the configuration files within the resource package¹ submitted for running our method.

5.2. Experimental Comparison and Analysis

To validate the effectiveness of our approach, we design a set of experimental settings that include not only our complete method but also ablation and comparison settings as follows:

- *DeepHE3*[6]. This experimental setting evaluates the performance of using only the DeepHE3 architecture to predict Hamiltonians. DeepHE3 will serve as the first-stage network in implementation of our framework in the following experiments. Although our first regression stage is designed with the flexibility to employ any combination of operators with prior $SO(3)$ -equivariance, for a clear and fair comparison, we here opt to use the architecture of DeepHE3 which consists of node and edge encoders with comprehensive priorly $SO(3)$ -equivariant operators [20, 5], under the same hyperparameters from their open source resources ², ensuring our experimental results can be reliably compared to the established SOTA method. Notably, the results of DeepHE3 reproduced with its latest resources are slightly better than those reported in their original paper [6].

- *Stage1_{DeepHE3} + Stage2_{DeepHE3}*: This experimental setting arranges two DeepHE3 networks as a two-stage cascaded regression framework for Hamiltonian prediction.

- *GFormer*. This experimental setting evaluates the performance of using only the proposed non-linear graph Transformer (abbreviated as *GFormer*) architecture to predict Hamiltonians. The Transformer network will serve as the second-stage network in subsequent experimental settings. To facilitate the empirical learning of $SO(3)$ -equivariance for non-linear modules, rigid rotational data augmentation on the training samples is introduced.

- *Stage1_{GFormer} + Stage2_{GFormer}*. This experimental setting arranges two of the non-linear graph Transformer networks as a cascaded regression framework for Hamiltonian prediction.

²<https://github.com/Xiaoxun-Gong/DeepH-E3>

- $Stage1_{DeepHE3} + Stage2_{GFormer}^{-cas}$: This experimental setting retains the two-stage framework, only removing the cascaded regression strategy at the output level by directly taking the second stage to predict the entire Hamiltonian targets. This setup is used to exactly examine the necessity of the cascaded regression strategy, thus only removing the prediction results of the first stage network at the output level, while retaining the first stage’s support for the second stage at the feature level. This aspect makes it different from the previous setups, i.e., $GFormer$ and $Stage1_{GFormer} + Stage2_{GFormer}$, where the non-linear Transformer operates independently in the feature encoding phase as well.

- $Stage1_{DeepHE3} + Stage2_{GFormer}^{-cov}$: This experimental setting retains the two-stage framework with cascaded regression mechanism, only removing the mechanism of integrating features with prior covariance into the input layers of Transformer blocks in the second stage. This setup is used to examine the necessity of these covariant features in assisting the non-linear graph Transformer network at capturing $SO(3)$ -equivariance.

- $Stage1_{DeepHE3} + Stage2_{GFormer}^{-att}$: This experimental setting retains the two-stage framework and their corporation at both feature level as well as output level, only removing the attention mechanism from the Transformer and replacing it by mixing neighboring features by stationary averages similar to DeepHE3. This setup is used to examine the necessity of the multi-head attention mechanism.

- $Ours@(Stage1_{DeepHE3} + Stage2_{GFormer})$: An implementation of our whole framework with mechanisms of DeepHE3 as well as the proposed graph Transformer respectively serve as the two feature encoding and target regres-

sion stages.

Experimental results of our complete method as well as the compared experimental settings on the six benchmark databases are presented in Table 2, 3, and 4, respectively detailing the results for monolayer structures, as well as the the results for non-twisted and twisted samples of bilayer structures. In these tables, the Mean Absolute Error (MAE) metric is used as the accuracy metric. Besides the classical MAE metric, denoted as MAE_{all} , which measures the average error among all testing samples, the MAE on the most challenging sample with worst accuracy from each database is also a crucial metric. We record it as MAE_{cha} , to distinguish it from MAE_{all} . To offset the randomness of experiments, we conduct independent experiments for 10 times repeatedly and report MAE_{all} and MAE_{cha} , averaged across these 10 experiments. We also report the standard deviation ($\pm\sigma$), a bar measuring the statistical fluctuation of the experimental results in these tables.

In addition to taking the Hamiltonian of each edge as a whole for accuracy statistics, since the Hamiltonian matrix in the direct product state is constituted by several basic blocks based on the angular momentum of interacting orbitals, we also conduct fine-grained accuracy statistics on these basic blocks. The MAE metrics (denoted as MAE_{block}) of our method and DeepHE3 on different blocks of the Hamiltonian matrix of the six structures are presented in Fig. 3 and 4, where Fig. 3 illustrates the results on monolayer structures, while Fig. 4 is dedicated to the bilayer structures. These results of MAE_{block} in these tables are gathered from the mean of 10 independent experiments.

From these tables and figures, we find that the proposed hybrid approach

Table 2: Comparison of experimental results on the monolayer structures. Both the mean and standard deviation of MAE_{all} as well as MAE_{cha} (/meV) from 10 independent repeated experiments are provided.

| Dataset | Method | MAE_{all} | MAE_{cha} |
|---------|---|-------------------------------------|-------------------------------------|
| MG | <i>DeepHE3</i> | 0.251 ± 0.002 | 0.357 ± 0.002 |
| | <i>Stage1_{DeepHE3} + Stage2_{DeepHE3}</i> | 0.239 ± 0.003 | 0.338 ± 0.003 |
| | <i>GFormer</i> | 0.816 ± 0.005 | 0.897 ± 0.005 |
| | <i>Stage1_{GFormer} + Stage2_{GFormer}</i> | 0.653 ± 0.004 | 0.720 ± 0.005 |
| | <i>Stage1_{DeepHE3} + Stage2_{GFormer}^{-cas}</i> | 0.774 ± 0.005 | 0.880 ± 0.006 |
| | <i>Stage1_{DeepHE3} + Stage2_{GFormer}^{-cov}</i> | 0.243 ± 0.001 | 0.328 ± 0.002 |
| | <i>Stage1_{DeepHE3} + Stage2_{GFormer}^{-att}</i> | 0.221 ± 0.002 | 0.297 ± 0.001 |
| | <i>Ours@(Stage1_{DeepHE3} + Stage2_{GFormer})</i> | 0.176 ± 0.001 | 0.267 ± 0.001 |
| MM | <i>DeepHE3</i> | 0.406 ± 0.002 | 0.574 ± 0.003 |
| | <i>Stage1_{DeepHE3} + Stage2_{DeepHE3}</i> | 0.392 ± 0.001 | 0.499 ± 0.002 |
| | <i>GFormer</i> | 1.025 ± 0.004 | 1.250 ± 0.004 |
| | <i>Stage1_{GFormer} + Stage2_{GFormer}</i> | 0.911 ± 0.003 | 0.923 ± 0.004 |
| | <i>Stage1_{DeepHE3} + Stage2_{GFormer}^{-cas}</i> | 0.927 ± 0.004 | 0.958 ± 0.003 |
| | <i>Stage1_{DeepHE3} + Stage2_{GFormer}^{-cov}</i> | 0.384 ± 0.002 | 0.414 ± 0.002 |
| | <i>Stage1_{DeepHE3} + Stage2_{GFormer}^{-att}</i> | 0.319 ± 0.001 | 0.366 ± 0.002 |
| | <i>Ours@(Stage1_{DeepHE3} + Stage2_{GFormer})</i> | 0.233 ± 0.001 | 0.293 ± 0.002 |

Table 3: Experimental results on the non-twisted subsets (marked with superscripts *nt*) of the bilayer structures.

| Dataset | Method | MAE_{all} | MAE_{cha} |
|------------------|--|-------------------------------------|-------------------------------------|
| BG ^{nt} | <i>DeepHE3</i> | 0.389 ± 0.002 | 0.453 ± 0.003 |
| | <i>Stage1</i> _{DeepHE3} + <i>Stage2</i> _{DeepHE3} | 0.372 ± 0.001 | 0.434 ± 0.002 |
| | <i>GFormer</i> | 1.295 ± 0.005 | 1.483 ± 0.004 |
| | <i>Stage1</i> _{GFormer} + <i>Stage2</i> _{GFormer} | 0.786 ± 0.005 | 0.828 ± 0.005 |
| | <i>Stage1</i> _{DeepHE3} + <i>Stage2</i> _{GFormer} ^{-cas} | 0.854 ± 0.003 | 0.920 ± 0.004 |
| | <i>Stage1</i> _{DeepHE3} + <i>Stage2</i> _{GFormer} ^{-cov} | 0.365 ± 0.002 | 0.427 ± 0.002 |
| | <i>Stage1</i> _{DeepHE3} + <i>Stage2</i> _{GFormer} ^{-att} | 0.348 ± 0.001 | 0.419 ± 0.003 |
| | <i>Ours</i> @(<i>Stage1</i> _{DeepHE3} + <i>Stage2</i> _{GFormer}) | 0.287 ± 0.002 | 0.362 ± 0.002 |
| BB ^{nt} | <i>DeepHE3</i> | 0.274 ± 0.003 | 0.304 ± 0.002 |
| | <i>Stage1</i> _{DeepHE3} + <i>Stage2</i> _{DeepHE3} | 0.268 ± 0.004 | 0.292 ± 0.003 |
| | <i>GFormer</i> | 0.886 ± 0.004 | 0.949 ± 0.005 |
| | <i>Stage1</i> _{GFormer} + <i>Stage2</i> _{GFormer} | 0.785 ± 0.004 | 0.816 ± 0.004 |
| | <i>Stage1</i> _{DeepHE3} + <i>Stage2</i> _{GFormer} ^{-cas} | 0.802 ± 0.003 | 0.873 ± 0.004 |
| | <i>Stage1</i> _{DeepHE3} + <i>Stage2</i> _{GFormer} ^{-cov} | 0.249 ± 0.004 | 0.281 ± 0.004 |
| | <i>Stage1</i> _{DeepHE3} + <i>Stage2</i> _{GFormer} ^{-att} | 0.243 ± 0.001 | 0.286 ± 0.003 |
| | <i>Ours</i> @(<i>Stage1</i> _{DeepHE3} + <i>Stage2</i> _{GFormer}) | 0.172 ± 0.001 | 0.198 ± 0.002 |
| BT ^{nt} | <i>DeepHE3</i> | 0.447 ± 0.001 | 0.480 ± 0.002 |
| | <i>Stage1</i> _{DeepHE3} + <i>Stage2</i> _{DeepHE3} | 0.435 ± 0.002 | 0.471 ± 0.002 |
| | <i>GFormer</i> | 1.018 ± 0.005 | 1.230 ± 0.006 |
| | <i>Stage1</i> _{GFormer} + <i>Stage2</i> _{GFormer} | 0.903 ± 0.003 | 0.982 ± 0.005 |
| | <i>Stage1</i> _{DeepHE3} + <i>Stage2</i> _{GFormer} ^{-cas} | 0.930 ± 0.004 | 1.026 ± 0.004 |
| | <i>Stage1</i> _{DeepHE3} + <i>Stage2</i> _{GFormer} ^{-cov} | 0.439 ± 0.001 | 0.466 ± 0.003 |
| | <i>Stage1</i> _{DeepHE3} + <i>Stage2</i> _{GFormer} ^{-att} | 0.385 ± 0.001 | 0.414 ± 0.002 |
| | <i>Ours</i> @(<i>Stage1</i> _{DeepHE3} + <i>Stage2</i> _{GFormer}) | 0.294 ± 0.002 | 0.321 ± 0.002 |
| BS ^{nt} | <i>DeepHE3</i> | 0.397 ± 0.003 | 0.424 ± 0.001 |
| | <i>Stage1</i> _{DeepHE3} + <i>Stage2</i> _{DeepHE3} | 0.389 ± 0.002 | 0.410 ± 0.002 |
| | <i>GFormer</i> | 1.352 ± 0.005 | 1.483 ± 0.005 |
| | <i>Stage1</i> _{GFormer} + <i>Stage2</i> _{GFormer} | 0.862 ± 0.005 | 0.922 ± 0.004 |
| | <i>Stage1</i> _{DeepHE3} + <i>Stage2</i> _{GFormer} ^{-cas} | 0.898 ± 0.005 | 0.960 ± 0.005 |
| | <i>Stage1</i> _{DeepHE3} + <i>Stage2</i> _{GFormer} ^{-cov} | 0.392 ± 0.002 | 0.401 ± 0.001 |
| | <i>Stage1</i> _{DeepHE3} + <i>Stage2</i> _{GFormer} ^{-att} | 0.348 ± 0.002 | 0.375 ± 0.003 |
| | <i>Ours</i> @(<i>Stage1</i> _{DeepHE3} + <i>Stage2</i> _{GFormer}) | 0.282 ± 0.002 | 0.308 ± 0.002 |

Table 4: Experimental results on the twisted subsets (marked with superscripts t) of the bilayer structures.

| Dataset | Method | MAE_{all} | MAE_{cha} |
|-----------------|---|----------------------|----------------------|
| BG ^t | <i>DeepHE3</i> | 0.264 ± 0.003 | 0.429 ± 0.003 |
| | <i>Stage1_{DeepHE3} + Stage2_{DeepHE3}</i> | 0.257 ± 0.002 | 0.423 ± 0.003 |
| | <i>GFormer</i> | 0.982 ± 0.005 | 1.153 ± 0.006 |
| | <i>Stage1_{GFormer} + Stage2_{GFormer}</i> | 0.841 ± 0.004 | 0.873 ± 0.004 |
| | <i>Stage1_{DeepHE3} + Stage2_{GFormer}^{-cas}</i> | 0.801 ± 0.005 | 0.863 ± 0.004 |
| | <i>Stage1_{DeepHE3} + Stage2_{GFormer}^{-cov}</i> | 0.312 ± 0.003 | 0.441 ± 0.004 |
| | <i>Stage1_{DeepHE3} + Stage2_{GFormer}^{-att}</i> | 0.278 ± 0.002 | 0.428 ± 0.002 |
| | <i>Ours@(Stage1_{DeepHE3} + Stage2_{GFormer})</i> | 0.227 ± 0.002 | 0.403 ± 0.001 |
| BB ^t | <i>DeepHE3</i> | 0.468 ± 0.003 | 0.602 ± 0.004 |
| | <i>Stage1_{DeepHE3} + Stage2_{DeepHE3}</i> | 0.460 ± 0.003 | 0.595 ± 0.004 |
| | <i>GFormer</i> | 1.784 ± 0.006 | 1.921 ± 0.006 |
| | <i>Stage1_{GFormer} + Stage2_{GFormer}</i> | 1.426 ± 0.005 | 1.680 ± 0.006 |
| | <i>Stage1_{DeepHE3} + Stage2_{GFormer}^{-cas}</i> | 1.213 ± 0.004 | 1.569 ± 0.005 |
| | <i>Stage1_{DeepHE3} + Stage2_{GFormer}^{-cov}</i> | 0.530 ± 0.004 | 0.697 ± 0.004 |
| | <i>Stage1_{DeepHE3} + Stage2_{GFormer}^{-att}</i> | 0.504 ± 0.004 | 0.669 ± 0.005 |
| | <i>Ours@(Stage1_{DeepHE3} + Stage2_{GFormer})</i> | 0.438 ± 0.003 | 0.578 ± 0.002 |
| BT ^t | <i>DeepHE3</i> | 0.831 ± 0.003 | 0.850 ± 0.003 |
| | <i>Stage1_{DeepHE3} + Stage2_{DeepHE3}</i> | 0.826 ± 0.002 | 0.843 ± 0.002 |
| | <i>GFormer</i> | 2.682 ± 0.004 | 2.827 ± 0.006 |
| | <i>Stage1_{GFormer} + Stage2_{GFormer}</i> | 2.190 ± 0.003 | 2.379 ± 0.004 |
| | <i>Stage1_{DeepHE3} + Stage2_{GFormer}^{-cas}</i> | 1.892 ± 0.003 | 1.937 ± 0.004 |
| | <i>Stage1_{DeepHE3} + Stage2_{GFormer}^{-cov}</i> | 0.928 ± 0.004 | 0.943 ± 0.004 |
| | <i>Stage1_{DeepHE3} + Stage2_{GFormer}^{-att}</i> | 0.837 ± 0.003 | 0.846 ± 0.003 |
| | <i>Ours@(Stage1_{DeepHE3} + Stage2_{GFormer})</i> | 0.774 ± 0.002 | 0.794 ± 0.003 |
| BS ^t | <i>DeepHE3</i> | 0.370 ± 0.001 | 0.390 ± 0.002 |
| | <i>Stage1_{DeepHE3} + Stage2_{DeepHE3}</i> | 0.358 ± 0.001 | 0.381 ± 0.002 |
| | <i>GFormer</i> | 1.785 ± 0.004 | 2.037 ± 0.005 |
| | <i>Stage1_{GFormer} + Stage2_{GFormer}</i> | 1.624 ± 0.004 | 1.953 ± 0.004 |
| | <i>Stage1_{DeepHE3} + Stage2_{GFormer}^{-cas}</i> | 1.569 ± 0.003 | 1.892 ± 0.005 |
| | <i>Stage1_{DeepHE3} + Stage2_{GFormer}^{-cov}</i> | 0.415 ± 0.003 | 0.456 ± 0.003 |
| | <i>Stage1_{DeepHE3} + Stage2_{GFormer}^{-att}</i> | 0.392 ± 0.002 | 0.421 ± 0.002 |
| | <i>Ours@(Stage1_{DeepHE3} + Stage2_{GFormer})</i> | 0.336 ± 0.001 | 0.365 ± 0.002 |

significantly improves the prediction accuracy beyond what is achievable solely with the parameter-independently SO(3)-equivariant mechanisms in *DeepHE3* or the non-linear mechanisms in *GFormer*, demonstrating the effectiveness on leveraging the complementarity of the two categories of neural mechanisms to overcome their respective challenges comprehensively analyzed in previous sections. On one hand, the highly expressive non-linear mechanisms in the Transformer effectively compensate for the limitations in non-linear expressiveness of *DeepHE3*'s mechanisms, thus lowering down the MAE_{all} of *DeepHE3* by a relative ratio of 29.88%, 42.61%, 26.22%, 37.23%, 34.23%, 28.97%, 14.02%, 6.41%, 6.86%, and 9.19%, on *MG*, *MM*, *BG^{nt}*, *BB^{nt}*, *BT^{nt}*, *BS^{nt}*, *BG^t*, *BB^t*, *BT^t* and *BS^t*, respectively; and lowering down MAE_{cha} by 25.21%, 48.95%, 20.09%, 34.87%, 33.13%, 27.36%, 6.06%, 3.99%, 6.59%, and 6.41%, on the respective datasets; and achieving better results in the vast majority of basic blocks, especially for the blocks where *DeepHE3* performs the worst, by reducing MAE_{block} of these challenging blocks by 13.89%, 66.36%, 29.69%, 39.42%, 33.81%, 28.74%, 13.11%, 10.83%, 5.03% and 7.95%, on the respective datasets, from which the MAE_{block} of challenging blocks in *MM*, *BG^{nt}* and *BT^{nt}* are surprisingly lowering down to within $1mev$. On the other hand, the mechanisms of *DeepHE3* help the non-linear mechanisms in the Transformer to better learn equivariance from the data and reduces the difficulty for the Transformer on regressing SO(3)-equivariant targets, thus also significantly promoting the results from merely using the Transformer network. From the experimental results, it is observed that without any prior information on covariance, solely relying on the non-linear Transformer architecture to learn SO(3)-equivariance from data

is extremely challenging despite rotational augmentation, due to the complexity and high-dimensionality nature of Hamiltonians as shown in Table 1. And since $SO(3)$ -equivariance is strongly linked to the intrinsic mathematical structure of Hamiltonians, the weakness on capturing $SO(3)$ -equivariance results in inadequate modeling of Hamiltonians, leading to inaccurate predictions, especially for samples that exhibit obvious $SO(3)$ -equivariant effects, such as twisted samples. Our framework addresses this challenge by incorporating mechanisms with prior covariance, which helps the non-linear mechanisms in the Transformer to learn equivariance from the data and reduces the difficulty for non-linear regression of $SO(3)$ -equivariant targets, bringing satisfactory performance of the non-linear modules. The results on twisted samples demonstrate that, our method, despite the extensive use of non-linear operators, can still capture the symmetry properties of Hamiltonians and make equivariant predictions under rotational operations. In contrast to this, the experimental results from $Stage1_{DeepHE3} + Stage2_{DeepHE3}$ and $Stage1_{GFormer} + Stage2_{GFormer}$ shows that simply scaling up the parameters for $DeepHE3$ or $GFormer$ and fine-tuning it alone only yields limited improvements. This indicates that the bottlenecks encountered by these two categories of neural mechanisms might not be fully overcome through scaling up their sizes, further highlighting the superiority and necessity of our hybrid strategy.

As fine-grained ablation studies, by comparing the results of the three experimental settings, i.e., $Stage1_{DeepHE3} + Stage2_{GFormer}^{-cas}$, $Stage1_{DeepHE3} + Stage2_{GFormer}^{-cov}$, and $Stage1_{DeepHE3} + Stage2_{GFormer}^{-att}$, with our complete method, we could observe that the cascaded regression mechanism, the covariant fea-

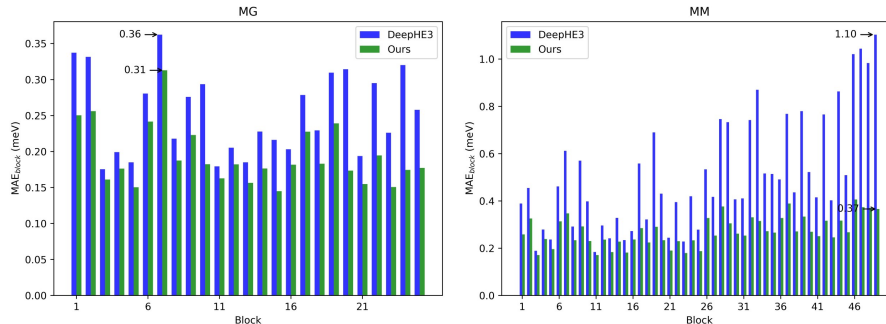


Figure 3: The MAE values (denoted as MAE_{block}) on various basic blocks of the Hamiltonian matrix in direct product state on the experimental monolayer structures.

ture integration mechanism, as well the multi-head attention mechanism, all contribute significantly to the performance of our method. The cascaded regression mechanism, by reducing the output space of the non-linear network, eases the difficulties on non-linear regression of Hamiltonians with $SO(3)$ -equivariance; the covariant feature integration mechanism, through leveraging theoretical-guaranteed covariant features from DeepHE3 and geometric knowledge, successfully assists the non-linear network in learning $SO(3)$ -equivariance; the multi-head attention mechanism, by assigning dynamic weights when fusing features, adapts to the wide variation range of geometric conditions, including both thermal deformations and twists. Under the novel combination of these mechanisms, networks from the two stage complement each other effectively, making our framework possess both excellent expressive capability and $SO(3)$ -equivariant performance to achieve good results.

Among current deep learning studies on Hamiltonians modeling, the DeepH series have conducted comprehensive experiments on various types of

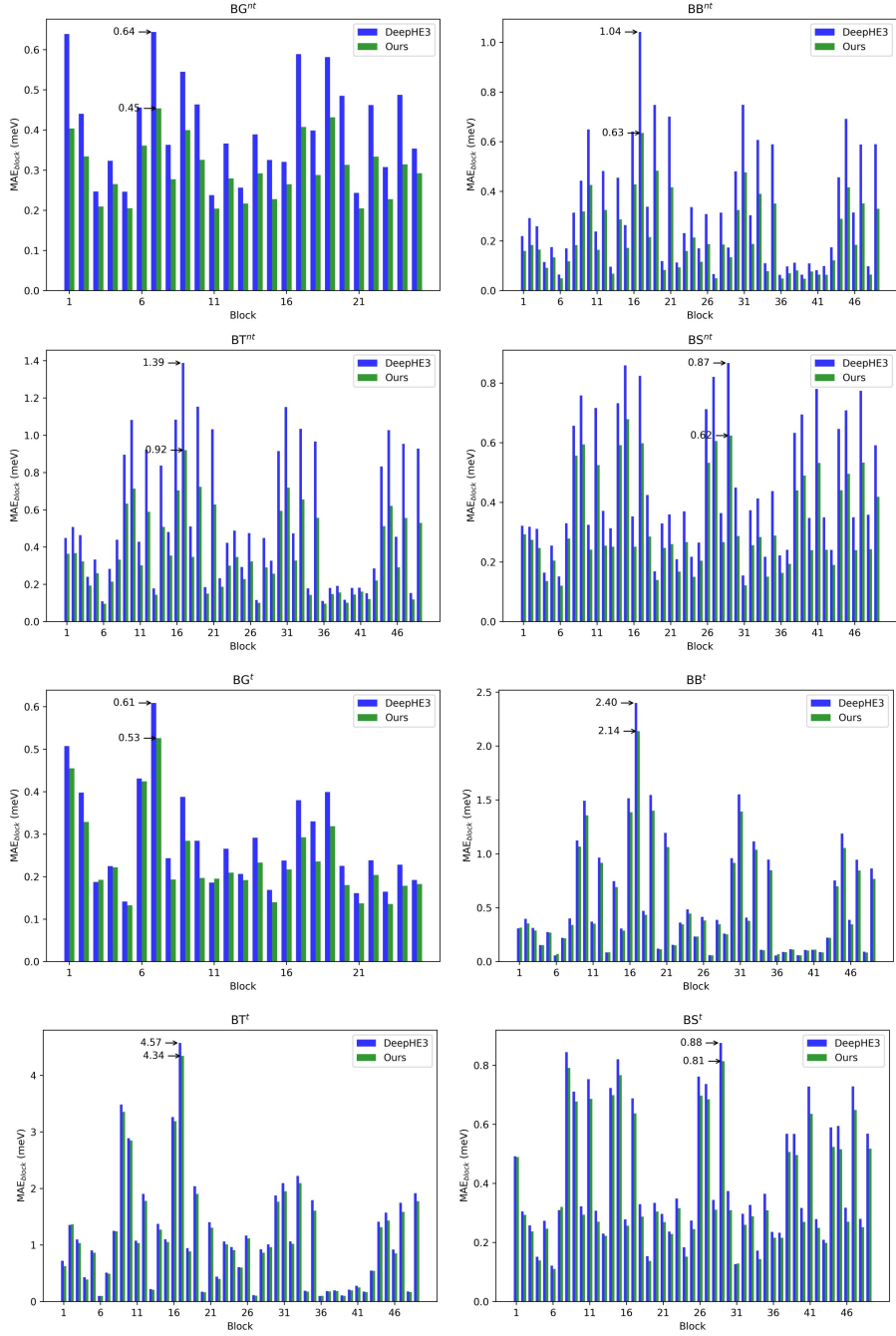


Figure 4: The MAE values (denoted as MAE_{block}) on various basic blocks of the Hamiltonian matrix in direct product state on the non-twisted (marked with superscripts nt) and twisted (marked with superscripts t) bilayer structures.

atomic structures, proving the SOTA performance. The paper of DeepHE3 has demonstrated it to surpass DeepH in accuracy by integrating neural mechanisms with prior equivariance; and since our method effectively harmonizes $\text{SO}(3)$ -equivariance and expressiveness of deep neural networks, we further surpass DeepHE3 in all of the benchmark databases, both on average and for the most challenging samples and blocks, both on non-twisted and twisted samples, conforming the leading performance in the field of deep Hamiltonian regression.

6. Time Complexity

The time complexity for both the first-stage and the second-stage networks is $\mathcal{O}(BN\bar{E})$, where B is the number of their basic blocks, N is the total number of atoms in a system, and \bar{E} is the average number of neighboring atoms within the cutoff radius of a given atom. When N is small, the system forms edges between each pair of atoms, and \bar{E} is approximately equal to N . However, as N increases to a large value, due to the locality of the Hamiltonian, the set of neighboring atoms for an atom typically remains roughly stable, so \bar{E} is roughly a constant and does not significantly increase with the growth of N . Therefore, for big atomic systems with very large N , $\bar{E} \ll N$, and similarly, $B \ll N$. In this case, the time complexity of our framework tends towards $\mathcal{O}(N)$. In contrast, for the traditional DFT method [11], which requires T rounds of iterative decomposition of $N \times N$ matrices, the time complexity is $\mathcal{O}(TN^3)$. As N increases, the cubic complexity of N results in significant computational overhead, and to achieve self-consistency, T is usually very large, exacerbating the computational burden, leading to difficulties for simulations of large atomic systems within an acceptable time

frame. On the contrary, our framework offers an efficient pathway for simulating large atomic systems with linear time complexity of N and without the need for T rounds of iterations.

7. Conclusion

Deep learning for regressing electronic structure Hamiltonian requires adherence to covariance laws, facing a pivotal challenge to achieve $\text{SO}(3)$ -equivariance without compromising neural expressiveness. To solve this, we make an exploration towards highly-expressive $\text{SO}(3)$ -equivariant deep learning by proposing a hybrid two-stage regression framework, where the first stage employs neural mechanisms inherent with $\text{SO}(3)$ -equivariance properties prior to the learning process based on group theory, yielding baseline Hamiltonians with series of equivariant features assisting the subsequent stage on capturing $\text{SO}(3)$ -equivariance. The second stage, leveraging the proposed non-linear 3D graph Transformer network for fine-grained structural analysis of 3D atomic systems, learns $\text{SO}(3)$ -equivariant patterns from training data with the help of the first stage, while in turn, refines the initial Hamiltonian predictions via enhanced network expressiveness. Such a combination allows for accurate, generalizable Hamiltonian predictions while upholding strong $\text{SO}(3)$ -equivariance against rotational transformations. Our methodology demonstrates SOTA performance in Hamiltonian prediction, validated through six benchmark databases, showing good potentials in high-performance simulation of atomic systems.

8. Acknowledgements

This work was supported by the National Natural Science Foundation of China (Grant Number 12134012) and the Strategic Priority Research Program of Chinese Academy of Sciences (Grant Number XDB0500201).

References

- [1] Cao, Y., Fatemi, V., Fang, S., Watanabe, K., Taniguchi, T., Kaxiras, E., Jarillo-Herrero, P., 2018. Unconventional superconductivity in magic-angle graphene superlattices. *Nature* 556, 43–50.
- [2] Cohen, T.S., Welling, M., 2017. Steerable cnns, in: ICLR.
- [3] Dieleman, S., Fauw, J.D., Kavukcuoglu, K., 2016. Exploiting cyclic symmetry in convolutional neural networks, in: ICML Workshop, pp. 1889–1898.
- [4] Fuchs, F., Worrall, D.E., Fischer, V., Welling, M., 2020. Se(3)-transformers: 3d roto-translation equivariant attention networks, in: NeurIPS.
- [5] Geiger, M., Smidt, T.E., 2022. e3nn: Euclidean neural networks. CoRR abs/2207.09453.
- [6] Gong, X., Li, H., Zou, N., Xu, R., Duan, W., Xu, Y., 2023. General framework for e (3)-equivariant neural network representation of density functional theory hamiltonian. *Nature Communications* 14, 2848.

- [7] Gu, Q., Zhang, L., Feng, J., 2022. Neural network representation of electronic structure from ab initio molecular dynamics. *Science Bulletin* 67, 29–37.
- [8] He, M., Cai, J., Zheng, H., Seewald, E., Taniguchi, T., Watanabe, K., Yan, J., Yankowitz, M., Pasupathy, A., Yao, W., et al., 2024. Dynamically tunable moiré exciton rydberg states in a monolayer semiconductor on twisted bilayer graphene. *Nature Materials* .
- [9] Hohenberg, P., Kohn, W., 1964. Inhomogeneous electron gas. *Physical Review* 136, B864.
- [10] Jaderberg, M., Simonyan, K., Zisserman, A., Kavukcuoglu, K., 2015. Spatial transformer networks, in: *NeurIPS*, pp. 2017–2025.
- [11] Kohn, W., Sham, L.J., 1965. Self-consistent equations including exchange and correlation effects. *Physical Review* 140, A1133.
- [12] Kondor, R., Son, H.T., Pan, H., Anderson, B.M., Trivedi, S., 2018. Covariant compositional networks for learning graphs, in: *ICLR Workshop*.
- [13] Li, H., Wang, Z., Zou, N., Ye, M., Xu, R., Gong, X., Duan, W., Xu, Y., 2022. Deep-learning density functional theory hamiltonian for efficient ab initio electronic-structure calculation. *Nature Computational Science* 2, 367–377.
- [14] Liao, Y., Smidt, T.E., 2023. Equiformer: Equivariant graph attention transformer for 3d atomistic graphs, in: *ICLR*.

- [15] Liao, Y., Wood, B.M., Das, A., Smidt, T.E., 2024. Equiformerv2: Improved equivariant transformer for scaling to higher-degree representations, in: ICLR.
- [16] Musaelian, A., Batzner, S., Johansson, A., Sun, L., Owen, C.J., Kornbluth, M., Kozinsky, B., 2023. Learning local equivariant representations for large-scale atomistic dynamics. *Nature Communications* 14.
- [17] Passaro, S., Zitnick, C.L., 2023. Reducing $SO(3)$ convolutions to $SO(2)$ for efficient equivariant gnns, in: ICML, pp. 27420–27438.
- [18] Ravanbakhsh, S., Schneider, J.G., Póczos, B., 2017. Equivariance through parameter-sharing, in: ICML, pp. 2892–2901.
- [19] Schütt, K.T., Gastegger, M., Tkatchenko, A., Müller, K.R., Maurer, R.J., 2019. Unifying machine learning and quantum chemistry with a deep neural network for molecular wavefunctions. *Nature Communications* 10, 5024.
- [20] Thomas, N., Smidt, T., Kearnes, S., Yang, L., Li, L., Kohlhoff, K., Riley, P., 2018. Tensor field networks: Rotation-and translation-equivariant neural networks for 3d point clouds. *arXiv preprint arXiv:1802.08219* .
- [21] Unke, O., Bogojeski, M., Gastegger, M., Geiger, M., Smidt, T., Müller, K.R., 2021. $Se(3)$ -equivariant prediction of molecular wavefunctions and electronic densities, pp. 14434–14447.
- [22] Wang, C., Zhang, X.W., Liu, X., He, Y., Xu, X., Ran, Y., Cao, T., Xiao, D., 2024. Fractional chern insulator in twisted bilayer mote 2. *Physical Review Letters* 132.

- [23] Wang, H., Zhang, L., Han, J., Weinan, E., 2018. Deepmd-kit: A deep learning package for many-body potential energy representation and molecular dynamics. *Computer Physics Communications* 228, 178–184.
- [24] Zhang, X., Wang, L., Helwig, J., Luo, Y., Fu, C., Xie, Y., Liu, M., Lin, Y., Xu, Z., Yan, K., Adams, K., Weiler, M., Li, X., Fu, T., Wang, Y., Yu, H., Xie, Y., Fu, X., Strasser, A., Xu, S., Liu, Y., Du, Y., Saxton, A., Ling, H., Lawrence, H., Stärk, H., Gui, S., Edwards, C., Gao, N., Ladera, A., Wu, T., Hofgard, E.F., Tehrani, A.M., Wang, R., Daigavane, A., Bohde, M., Kurtin, J., Huang, Q., Phung, T., Xu, M., Joshi, C.K., Mathis, S.V., Azizzadenesheli, K., Fang, A., Aspuru-Guzik, A., Bekkers, E., Bronstein, M., Zitnik, M., Anandkumar, A., Ermon, S., Lió, P., Yu, R., Günnemann, S., Leskovec, J., Ji, H., Sun, J., Barzilay, R., Jaakkola, T., Coley, C.W., Qian, X., Qian, X., Smidt, T., Ji, S., 2023. Artificial intelligence for science in quantum, atomistic, and continuum systems. arXiv preprint arXiv:2307.08423 .
- [25] Zhang, Y., Hu, C., Jiang, B., 2019. Embedded atom neural network potentials: Efficient and accurate machine learning with a physically inspired representation. *The journal of physical chemistry letters* 10, 4962–4967.
- [26] Zhang, Y., Jiang, B., 2023. Universal machine learning for the response of atomistic systems to external fields. *Nature Communications* 14.
- [27] Zhong, Y., Yu, H., Su, M., Gong, X., Xiang, H., 2023. Transferable equivariant graph neural networks for the hamiltonians of molecules and solids. *npj Computational Materials* 9, 182.

- [28] Zitnick, L., Das, A., Kolluru, A., Lan, J., Shuaibi, M., Sriram, A., Ulissi, Z.W., Wood, B.M., 2022. Spherical channels for modeling atomic interactions, in: NeurIPS.